

Two-dimensional structure in a generic model of triangular proteins and protein trimers

Philip J. Camp* and Peter D. Duncan

School of Chemistry, University of Edinburgh, West Mains Road, Edinburgh EH9 3JJ, United Kingdom

(Dated: February 6, 2022)

Motivated by the diversity and complexity of two-dimensional crystals formed by triangular proteins and protein trimers, we have investigated the structures and phase behavior of hard-disk trimers. In order to mimic specific binding interactions, each trimer possesses an ‘attractive’ disk which can interact with similar disks on other trimers *via* an attractive square-well potential. At low density and low temperature, the fluid phase mainly consists of tetramers, pentamers, or hexamers. Hexamers provide the structural motif for a high-density, low-temperature periodic solid phase, but we also identify a metastable periodic structure based on a tetramer motif. At high density there is a transition between orientationally ordered and disordered solid phases. The connections between simulated structures and those of 2D protein crystals – as seen in electron microscopy – are briefly discussed.

PACS numbers: 64.60.-i, 64.70.Dv, 05.10.Ln

I. INTRODUCTION

Two-dimensional (2D) materials present some fascinating challenges to condensed-matter theory, with even the most simple 2D systems harboring surprises. One of the most famous problems involves the precise description of melting in 2D solids made up of hard, disk-like particles with short-range repulsive interactions.^{1,2,3,4} Specifically, does the fluid undergo a weak first-order transition to the solid, or is there an intermediate hexatic phase linked by two continuous phase transitions? Related avenues of research concern the existence of exotic phases in systems made up of more complex particles, such as (non)periodic solids of hard-disk dimers,^{5,6} pentamers and hexamers,⁷ tetratic phases of hard squares⁸ and hard rectangles,⁹ and orientationally ordered solids of hard pentagons and heptagons.¹⁰ The effects of additional interactions on the phase behavior and dynamics of 2D systems are also of interest, as evidenced by recent studies on dipolar potentials in the context of magnetic colloids.¹¹ Such models provide an ideal testing ground for condensed-matter theories, and in some cases challenge our most fundamental understanding of the properties of matter.

Despite their simplicity, 2D models can provide reliable descriptions of some real, and rather complex, experimental situations. For example, in a number of recent studies, 2D models have been employed to help interpret and understand the clustering and crystallization of proteins at interfaces. The conformations and interactions of proteins are central to biological activity, and ideally one would like to investigate these properties *in vivo*. Unfortunately, structural information is most commonly obtained from X-ray diffraction studies on crystals. There is a class of proteins, however, that can be studied under conditions resembling those *in vivo*. Membrane proteins constitute a large class of molecules found within the lipid bilayers that constitute cell walls. They fulfill a variety of roles, such as controlling the selective

transport of ions and molecules across cell membranes, or providing binding sites for other molecules on to the membrane. The structures of membrane proteins can be studied by deposition on to a surface, alongside lipids, to form either low surface-coverages or 2D crystals; the hydrophobic lipids help to mimic the interior of the membrane. Electron microscopy or atomic-force microscopy can then be used to image directly the clustering and packing of proteins at the solid-air interface.¹² In many cases, the ordering of proteins can be rationalized on the basis of their gross shapes (the way in which those shapes would ‘tile the plane’) and the presence of specific binding interactions between domains on different molecules. For example, the surface structure of bacteriorhodopsin (a transmembrane protein) is comprised of a close-packed array of trimers, each made up of monomers that resemble 120° sectors of a circle. Monte Carlo (MC) simulations of hard sectors – with an additional attractive square-well potential to mimic specific binding interactions – yield insight on the self-assembly and subsequent crystallization processes.¹³ In another application, the ordering in 2D crystals of annexin V – another ‘triangular’ membrane protein – was reproduced in simulations of a hard-disk model decorated with an appropriate orientation-dependent potential to mimic the locations of the specific binding sites on the protein. Experimentally observed honeycomb and triangular structures were captured by the molecular model. These examples show that the basic physics of large-scale structural order in 2D protein crystals can be studied with simple models, and without resorting to atomistically detailed – and hence very expensive – computer simulations.

There are a large number of proteins which are either inherently triangular in shape, or otherwise form trimeric structures.^{14,15,16,17,18,19,20} For example, rotavirus inner capsid protein V6 forms trimers resembling equilateral triangles, which pack in 2D crystals (space group *p6*).¹⁴ Specific fragments of prion proteins found *in vivo* form trimeric units that crystallize in to a 2D structure (space

group $p3$).¹⁹ Finally, we highlight an example in which a membrane fusion protein (from the Semiliki forest virus) is seen to form pentagons of trimers, with the center of the pentagon raised slightly out of the plane.¹⁸ Some semblance of local five-fold coordination can also been seen in TetA – a roughly triangular transporter protein – at moderate surface coverages.¹⁶

Motivated by the diversity of 2D crystal structures exhibited by trimeric protein units, and also by the observation of five-fold coordination,¹⁸ we have investigated the structure and phase behavior of model trimeric molecules made up of hard disks. In order to mimic specific binding interactions, such as those that might give rise to local five-fold coordination, we focus on an equilateral triangle of three hard disks at contact, in which one disk can interact with the corresponding disks on other molecules *via* a short-range attractive square-well potential. As we will show below, this raises the possibility of generating orientational order within simple close-packed structures, and also offers the opportunity of forming clusters at low surface coverages. Using MC simulations, we map out the phase diagram of the model system, and characterize the structures of the low-density clustered fluid and high-density solids which are formed at low temperature. The remainder of the article is organized as follows. In Section II we describe the molecular model, and summarize the simulation methods. The results are presented in Section III, and Section IV concludes the paper.

II. MODEL AND METHODS

The molecular model consists of three hard disks, each of diameter σ , fused at mutual contact to form an equilateral triangle. Two of the disks on each molecule are purely repulsive, and interact with all other disks in the system through the potential

$$u(r) = \begin{cases} \infty & r < \sigma \\ 0 & r \geq \sigma \end{cases} \quad (1)$$

where r is the separation between the centers of two disks. The third disk on each molecule carries a central attractive interaction site; these ‘attractive’ disks interact with each other *via* the potential

$$u(r) = \begin{cases} \infty & r < \sigma \\ -\epsilon & \sigma \leq r < \lambda\sigma \\ 0 & r \geq \lambda\sigma \end{cases} \quad (2)$$

where $\lambda > 1$ controls the range of the attraction. This potential crudely mimics an effective attraction between vertices of the molecular triangles, which might arise through specific interactions (e.g. hydrogen bonding, disulfide bridges, effective solvophobic interactions).

The parameter λ will clearly have a crucial role to play in the thermodynamics of the system. If $\lambda \gg 1$ then one should anticipate a conventional phase diagram containing a vapor-liquid transition, and a fluid-solid transition. The orientation of a trimer can be defined by

a vector \mathbf{n} joining the geometrical center of the trimer with the center of the attractive disk. It is unlikely that there would be any periodic orientational ordering of \mathbf{n} in the solid phase; if two trimers can interact favorably irrespective of the mutual orientation, then on entropy grounds the orientations will be disordered. In the opposite extreme, $\lambda \gtrsim 1$, the molecules will feel the orientation dependence of the net trimer-trimer potential, and ultimately we might expect the vapor-liquid transition to disappear from the equilibrium phase diagram. Indeed, in a pure square-well hard-sphere fluid, condensation becomes metastable with respect to freezing when $\lambda < 1.25$.²¹ In the present case, an interaction range $\lambda < \sqrt{3}$ guarantees that attractive sites must face each other directly in order to interact; when $\lambda > \sqrt{3}$ it is possible for an attractive disk to be within interaction range of a trimer even if it approaches from ‘behind’. With these comments in mind, we have chosen to study a system with $\lambda = 1.25$. The ratio of $\lambda\sigma$ to the (angle-averaged) diameter of the trimer is smaller than that in a pure square-well hard-sphere system with the same value of λ , and assuming some sort of correspondence between two and three-dimensional systems, we do not anticipate there being a vapor-liquid transition in the equilibrium phase diagram. On the other hand, because the trimers have to attain quite specific mutual orientations in order to interact favorably (since $\lambda < \sqrt{3}$), we should expect to see some sort of non-trivial structure in fluid and solid phases at low temperatures.

Systems of $N = 120$ trimers were studied using MC simulations either in the isothermal-isobaric (NpT) ensemble or the canonical (NAT) ensemble.²² The simulation cell was rectangular with dimensions L_x and L_y , and area $A = L_x L_y$. Each MC cycle consisted of one translational trial move and one orientational trial move for each of N randomly selected molecules. To help equilibrate dense phases, every fifth MC cycle included N trial moves in which a randomly selected trimer was rotated by $\pm 120^\circ$. In NpT simulations of solid phases, L_x and L_y were varied independently; in NpT simulations of fluid phases, the simulation cell was constrained to be square. For most thermodynamic state points typical equilibration runs consisted of $\sim 10^5$ MC cycles, but some points (close to phase transitions) required $\sim 10^6$ MC cycles. Production runs were typically $\sim 10^5$ MC cycles. We define the following dimensionless units in terms of the square-well depth, ϵ , and the hard-disk diameter, σ : number density $\rho^* = N\sigma^2/A$; temperature $T^* = k_B T/\epsilon$; pressure $p^* = p\sigma^2/k_B T$.

III. RESULTS

The phase diagram of the model trimers in the density-temperature (ρ^*-T^*) plane is sketched in Fig. 1. Before detailing the determination of the phase boundaries, the characteristics of the different phases will be described. There are four distinct regions in the phase diagram. At

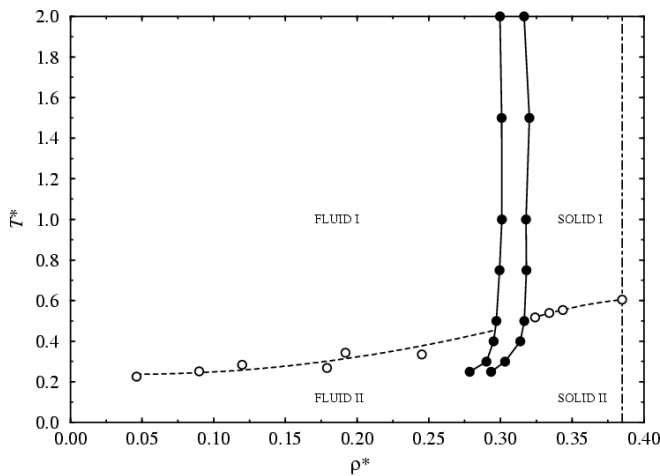


FIGURE 1

FIG. 1: Phase diagram of the model trimer system in the density-temperature (ρ^* - T^*) plane: (solid points and solid lines) approximate fluid-solid phase boundaries, assumed to be first order; (open points and dashed lines) boundaries between high-temperature unclustered states and low-temperature clustered states, as evidenced by maxima in the heat capacity along isobars; (dot-dashed line) close-packed density, $\rho_{cp}^* = 2/3\sqrt{3} \simeq 0.3849$.

low density and high temperature, a normal fluid phase is in evidence (fluid I). A typical simulation configuration is shown in Fig. 2(a). There is neither translational nor long-range orientational order in the system.

At high density and high temperature, the stable solid phase (solid I) possesses an orientationally disordered structure (in the sense that \mathbf{n} is disordered) with the trimers close-packed to form alternating rows displaced by $\sigma/2$. Figure 2(b) shows both the lack of orientational order, and the registry between alternating rows. Notice the black bonds showing how the disks are connected within the trimers; we call this an ‘AB’ structure to denote the alternating alignment of the rows. The close-packed rows resemble those formed by VP6,¹⁴ although the registry between the rows is different. At the end of this section, we will briefly discuss the possibility of solids with other close-packed structures.

At low temperature and low density we find a highly associated fluid (fluid II), in which the attractive disks aggregate to form distinct clusters. A typical configuration is shown in Fig. 2(c), which exhibits a broad distribution of cluster sizes. To identify clusters, we employ the obvious criterion that two trimers with attractive disks within interaction range belong to the same cluster. With this definition in mind, Fig. 2(c) shows that, in general, the attractive disks within the clusters form close-packed motifs, rather than loose arrangements of disks on the circumference of a ring. For clusters of three trimers there is no distinction, whereas for four or more trimers the close-packed arrangement is more favorable; in a ring, each disk would have two nearest neighbors, whereas close-packed motifs can accommodate more than two direct contacts.

In Fig. 3 we show the probability distribution function of clusters containing n molecules, at different pressures along an isotherm with $T^* = 0.3$. As the pressure and density increase, the distributions show peaks at progressively higher values of n . At the highest fluid-density shown – $\rho^* = 0.280$, Fig. 3(e) – the most probable cluster size is $n = 5$. We had hoped that these clusters would adopt a pentagonal structure, but instead the attractive disks form ‘Olympic rings’ motifs, such as those shown in Fig. 2(c). The maximum disk-disk separation in a perfect pentagon of disks is $\sqrt{2(1 - \cos 108^\circ)}\sigma \simeq 1.62\sigma$, which is longer than the range of the potential studied in this work. Hence, to minimize the energy, the cluster will contract to form a close-packed structure. Perhaps pentagonal clusters would be formed in a system with $1.62 \leq \lambda \leq \sqrt{3}$? (The upper limit means that there can be no other disks between two interacting attractive disks.) We did some test runs in the fluid phase with $\lambda = 1.7$, but no pentagonal clusters were observed. If anything, fewer distinct clusters were in evidence as compared to $\lambda = 1.25$, presumably because it is less crucial that the trimers attain a specific mutual orientation in order to interact.

Upon compression of the low-temperature fluid we often encountered metastable structures, such as that shown in Fig. 2(d). This clearly shows a predominance of $n = 6$ clusters, with the attractive disks close packed to form a parallelogram motif, but the clusters are not yet fully packed in to a solid structure. This process is completed upon further compression, to form a $p2$ periodic solid (solid II), a defective example of which is shown in Fig. 2(e). In simulations of the high-density solid II phase, the initial configuration consisted of the appropriate AB structure, but with \mathbf{n} for each molecule chosen randomly from the three molecular arms; the orientational structure shown in Fig. 2(e) develops spontaneously. The cluster distribution for such a solid at temperature $T^* = 0.3$ and density $\rho^* = 0.329$ is shown in Fig. 3(f). The primary peak is at $n = 6$, but the presence of defects – such as those shown in Fig. 2(e) – gives rise to smaller ‘clusters’ of attractive disks.

The fluid-solid phase boundaries were located by monitoring the equation of state $p(\rho)$ along selected isotherms in NpT simulations. For each isotherm, two sets of simulations were performed: a compression branch, starting from a low-density fluid configuration; and an expansion branch, starting from the perfect solid structure corresponding to that found in the compression branch at high pressure. Portions of two representative examples ($T^* = 0.3$ and $T^* = 1$) are shown in Fig. 4. Of course, the fluid equations of state extend to much lower densities, but these exhibit entirely conventional behavior and hence are not shown; in particular, there is no sign of a ‘van der Waals’ loop which would indicate a vapor-liquid phase transition. The main features of interest are the apparent discontinuities in the density at what are assumed to be first-order phase transitions (we will not open up the can of worms associ-

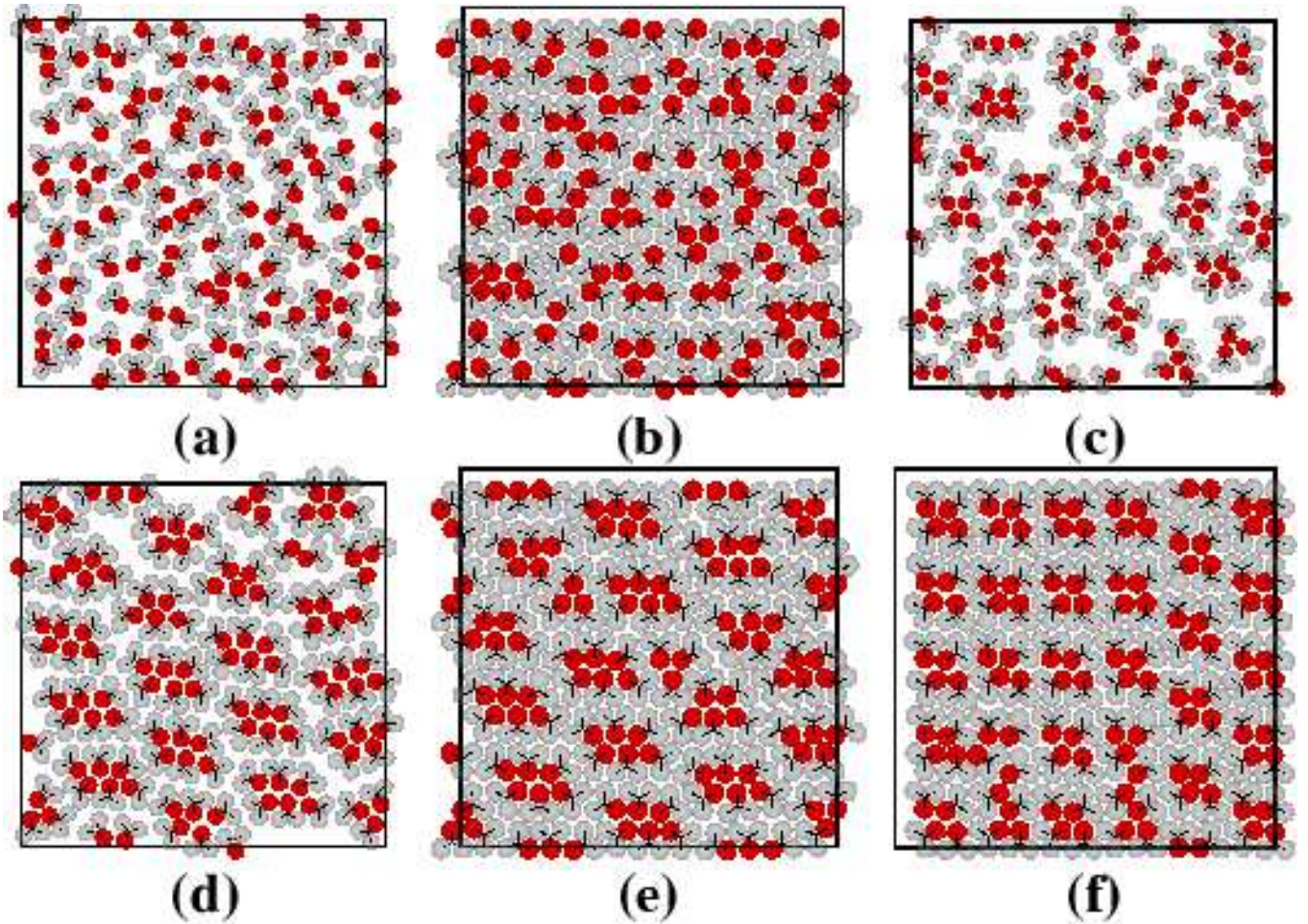


FIGURE 2

FIG. 2: (Color online) Configuration snapshots from NpT simulations: (a) normal fluid phase (fluid I) at $T^* = 2$, $p^* = 2.5$, $\rho^* = 0.259$; (b) orientationally disordered AB -solid phase (solid I) at $T^* = 2$, $p^* = 12$, $\rho^* = 0.345$; (c) clustered fluid phase (fluid II) at $T^* = 0.25$, $p^* = 0.75$, $\rho^* = 0.222$; (d) metastable state at $T^* = 0.25$, $p^* = 2.6$, $\rho^* = 0.290$; (e) orientationally ordered AB -solid phase (solid II) at $T^* = 0.25$, $p^* = 12$, $\rho^* = 0.349$; (f) metastable orientationally ordered AA -solid at $T^* = 0.25$, $p^* = 20$, $\rho^* = 0.356$. In each case the attractive disks are colored dark gray (red online), the repulsive disks are colored light gray, and all disks are drawn with diameter 1σ .

ated with the precise nature of two-dimensional melting and freezing^{1,2,3,4}). In Fig. 4 we indicate distinct fluid and solid branches in the equations of state, a number of putative metastable states (as discussed above), and approximate tie-lines connecting the fluid and solid coexistence densities, obtained as follows. The fluid branch was fitted with a virial expansion containing terms up to ρ^5 , i.e., $p/k_B T = \rho + \sum_{n=2}^5 B_n \rho^n$, while the solid branch was found to be fitted rather well by a simple van der Waals equation²³ of the form $p/k_B T = a\rho/(1 - b\rho) - c\rho^2$, which contains a free-volume term arising from repulsive interactions, and a mean-field term arising from the attractions. The coexistence densities were then estimated by extrapolating the fitted branches of the equation of state to a pressure half way between those in the highest-density stable fluid and the lowest-density stable solid;

the metastable states were identified as those that did not fit on to either branch and/or for which the simulation configuration was clearly neither pure solid nor pure fluid, e.g. Fig. 2(d). Obviously this approach provides only very rough locations for the phase boundaries shown in Fig. 1, but some general trends are nonetheless apparent. At very low temperatures, the coexistence densities decrease as the system is cooled, and the transition appears to be getting weaker. At high temperatures ($T \geq 1$) the fluid coexistence density ($\rho^* \simeq 0.30$) is very similar to the density at which the pure hard-disk fluid undergoes its transition, either to a hexatic or a solid (disk density $\rho^* = 0.899$,⁴ ‘trimer’ density $\rho^* = 0.300$). The apparent trimer solid coexistence density ($\rho^* \simeq 0.32$) is significantly larger than the melting density of hard disks (disk density $\rho^* \simeq 0.914$,⁴ ‘trimer’ density $\rho^* \simeq 0.305$).

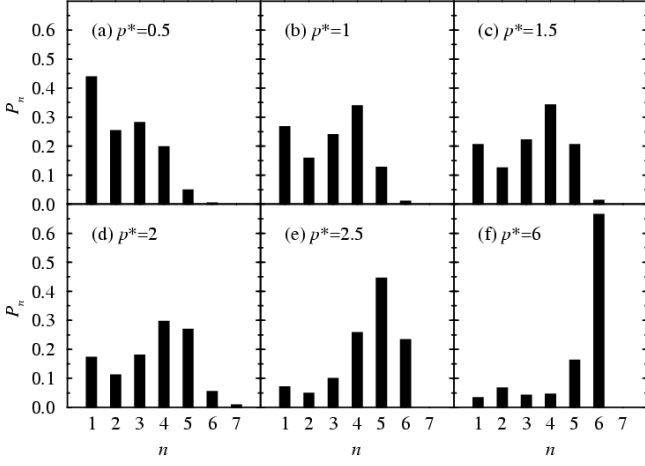


FIGURE 3

FIG. 3: Cluster distributions for systems along the isotherm $T^* = 0.3$: (a) $p^* = 0.5$, $\rho^* = 0.188$; (b) $p^* = 1$, $\rho^* = 0.230$; (c) $p^* = 1.5$, $\rho^* = 0.252$; (d) $p^* = 2$, $\rho^* = 0.265$; (e) $p^* = 2.5$, $\rho^* = 0.280$; (f) $p^* = 6$, $\rho^* = 0.329$. In (a)-(e) the system is fluid, whilst in (f) the system is solid (II).

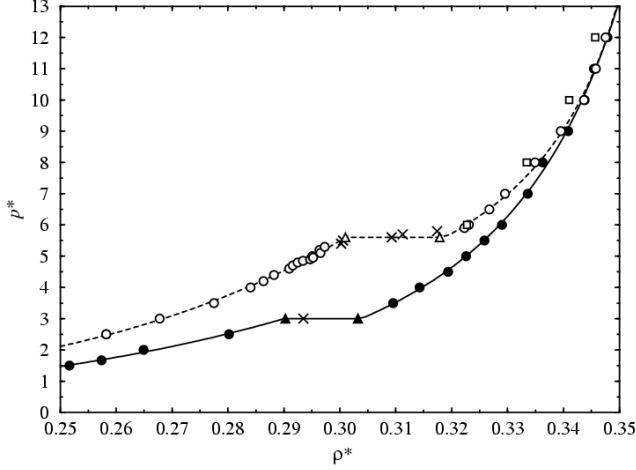


FIGURE 4

FIG. 4: Equations of state along isotherms with $T^* = 0.3$ (solid symbols, solid lines), and $T^* = 1$ (open symbols, dashed lines): (circles) state points from NpT simulations, with AB solid phases; (squares) state points from NpT simulations, with AA solid phases ($T^* = 1$ only); (crosses) putative metastable state points; (triangles) approximate coexistence densities; (lines) fits to the fluid and solid branches (see text). The statistical errors in the NpT simulation points are smaller than the symbols.

The final piece of the equilibrium phase diagram concerns the crossover from high-temperature orientationally disordered states to low-temperature states that possess structural motifs arising from the clustering of the attractive disks. To delineate the boundary between these two regimes, we calculated the heat capacity appropriate to the statistical mechanical ensemble being sampled. In general we used NpT simulations to measure $C_p = (\partial H / \partial T)_p$ – where $H = U + pA$ is the enthalpy

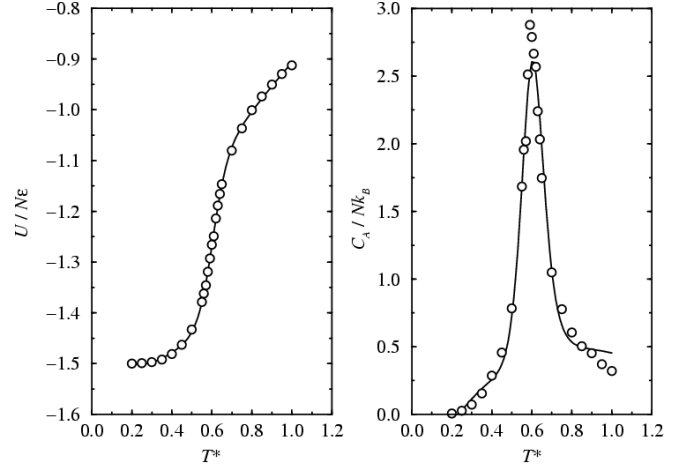


FIGURE 5

FIG. 5: Configurational energy U (left) and excess heat capacity C_A (right) as functions of reduced temperature T^* at the close-packed density $\rho^* = 2/3\sqrt{3} \simeq 0.3849$: (circles) simulation results; (lines) results derived from a Padé [5,5] fit (see text).

(minus the kinetic contribution) – as a function of temperature along an isobar. Since clustering must be accompanied by a drop in the configurational energy, and enthalpy, a peak in C_p would seem to be an obvious signal of a crossover from unclustered to clustered states. In simulations we evaluated the usual fluctuation formula, $C_p = [\langle H^2 \rangle - \langle H \rangle^2] / k_B T^2$, and, as a check, differentiated an $[n, n]$ Padé approximant fitted to the enthalpy as a function of T ;

$$H = \frac{a_0 + a_1 T + a_2 T^2 + \dots + a_n T^n}{1 + b_1 T + b_2 T^2 + \dots + b_n T^n}. \quad (3)$$

These two approaches yielded consistent results, and the peak in C_p was easy to locate accurately. In general the peak height is less pronounced at high densities, mainly due to the fact that even in the high-temperature phase there must be some attractive disks within interaction range due to the confinement. Thus, the most difficult situation obtains at close packing of the trimers, $\rho_{cp}^* = 2/3\sqrt{3}$. In this case we studied a perfect close-packed AB solid, and carried out NAT MC simulations with $\pm 120^\circ$ rotations only. We show results for the configurational energy, U , and the excess constant-area heat capacity, $C_A = (\partial U / \partial T)_A$, in Fig. 5. A [5,5] Padé fit provides a reliable description of the energy, and the corresponding results for C_A are consistent with those obtained *via* the fluctuation formula.

In Fig. 1 we show the positions of the maxima in C_p – and C_A at $\rho_{cp}^* = 2/3\sqrt{3}$ – along with separate cubic fits to the points in the fluid and solid regions of the phase diagram. It appears that the two branches would meet up somewhere in the fluid-solid coexistence region. We stress that the boundaries indicated do not represent thermodynamic phase transitions; rather, they separate different regimes of trimer association.

Finally, we briefly consider the possibility of the trimer system adopting other solid structures, such as the $p2$ AA structure shown in Fig. 2(f), in which the close-packed (horizontal) rows are matched with the neighboring rows. In this case, the low-temperature, orientationally ordered solid exhibits rhombic cluster-motifs containing only four attractive disks. Out of those four disks, two are interacting with two other disks, and two are interacting with three other disks. Hence, the minimum configurational energy for an AA solid is $-\frac{5}{4}\epsilon$ per trimer. In the AB structure, there are six attractive disks per parallelogram motif, of which two have two neighbors, two have three neighbors, and two have four neighbors, giving a minimum energy of $-\frac{3}{2}\epsilon$ per trimer. Hence, on energetic grounds, we should expect the AB structure to be thermodynamically favored. Even at high temperature, the AA structure appears to be less stable with respect to the AB structure. As an example, in Fig. 4, we show an AA -solid branch of the equation of state at $T^* = 1$, alongside the AB -solid branch. For a given pressure, the AB solid has the higher density which makes this state at least mechanically stable with respect to AA . Indeed, we only ever observed the fluid spontaneously freezing in to an AB structure. Although we have not performed free-energy calculations, it would be very surprising if an entropic effect could compensate for the relative energetic and mechanical stability of the AB phase with respect to the AA phase.

Another possible close-packed structure is illustrated in Fig. 6(a), without any indication of the attractive disks. This structure resembles that adopted by 2D crystals of TetA,¹⁶ although we never saw this packing structure emerge from our simulations. As far as our model is concerned, the absence of this structure at low temperature is easy to understand. In Figs. 6(b) and 6(c) we illustrate mirror images of the most obvious periodic arrangement of the attractive disks (space group $p3$). The energy per trimer is only -1ϵ , and so this is not competitive with the AB structure that is seen to emerge spontaneously in our simulations. Free-energy calculations would be of interest, particularly at high temperatures where entropy is everything!

IV. DISCUSSION

In this article we have described the structure and phase behavior of a generic model of trimeric molecules, largely motivated by recent experimental 2D microscopy studies of clustering and crystallization in triangular proteins and protein trimers. The molecular model consists of a triangle of hard disks, with one of the disks participating in attractive square-well interactions with similar disks on other trimers. The range of the square-well potential, $\lambda\sigma$, was 1.25 times the disk diameter. This system crudely mimics the general shape and specific interactions of a wide range of proteins. The model system exhibits fluid and solid phases which, at low tempera-

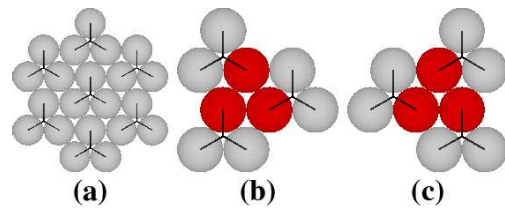


FIGURE 6

FIG. 6: (Color online) Illustrations of an alternative close-packed structure: (a) without an assignment of attractive disks; (b) and (c) mirror images of a possible structural motif for a periodic arrangement of attractive disks. The attractive disks are colored dark gray (red online), the repulsive disks are colored light gray, and all disks are drawn with diameter 1σ .

tures, possess interesting structural motifs arising from the clustering of the ‘attractive’ disks.

In the fluid, a distribution of clusters is in evidence, including tetramers, pentamers, and hexamers (of trimers). In the pentamers and hexamers, the attractive disks close-pack to form ‘Olympic rings’ and parallelogram shapes, respectively. We had hoped to find more open pentagonal clusters of trimers, such as those reported in Ref. 18. To investigate the formation of such clusters further, it might be interesting to study a system of hard isosceles triangles with the unique angle equal to 72° , and a short-range attraction operating between the corresponding vertices.

In the low-temperature solid, the basic structural motif consists of clusters of six molecules, with the attractive disks close-packed to form a parallelogram. A metastable solid possessing a motif made up of four molecules was also identified. The fundamental difference between the two situations is the registry between neighboring close-packed rows of trimers (AB versus AA). Even at high temperatures, the orientationally disordered AB solid is at least mechanically stable with respect to the AA solid. We identified a third structure based on hexagonal close packing, but this structure is not competitive either, at least in terms of energy. It would be worth performing free-energy calculations to study these issues further.

Finally, it is worth commenting that a diverse range of 2D structures can be generated from very simple molecular models. Fully atomistic calculations of 2D protein structures are expensive, and, it could be argued, yield little insight on the fundamental physics behind clustering and crystallization. As has been shown in a variety of cases, including the present study, the process of developing and studying simple models of complex systems can yield some surprising results.

Acknowledgments

The provision of a studentship for PDD by the Engineering and Physical Sciences Research Council (UK) is

gratefully acknowledged.

-
- * E-mail: philip.camp@ed.ac.uk
- ¹ J. M. Kosterlitz and D. J. Thouless, J. Phys. C.: Solid State Phys. **6**, 1181 (1973).
 - ² D. R. Nelson and B. I. Halperin, Phys. Rev. B **19**, 2457 (1979).
 - ³ A. P. Young, Phys. Rev. B **19**, 1855 (1979).
 - ⁴ K. Binder, S. Sengupta, and P. Nielaba, J. Phys.: Condens. Matter **14**, 2323 (2002).
 - ⁵ K. W. Wojciechowski, D. Frenkel, and A. C. Branka, Phys. Rev. Lett. **66**, 3168 (1991).
 - ⁶ K. W. Wojciechowski, Phys. Rev. B **46**, 26 (1992).
 - ⁷ K. W. Wojciechowski, K. V. Tretyakov, and M. Kowalik, Phys. Rev. E **67**, 036121 (2003).
 - ⁸ K. W. Wojciechowski and D. Frenkel, Comp. Methods in Science and Tech. **10**, 235 (2004).
 - ⁹ A. Donev, J. Burton, F. H. Stillinger, and S. Torquato, arxiv:cond-mat/0508550.
 - ¹⁰ T. Schilling, S. Pronk, B. Mulder, and D. Frenkel, Phys. Rev. E **71**, 036138 (2005).
 - ¹¹ J. J. Weis, J. Phys.: Condens. Matter **15**, S1471 (2003).
 - ¹² P. J. L. Werten, H.-W. Remigy, B. L. de Groot, D. Fotiadis, A. Philippsen, H. Strahlberg, H. Grubmüller, and A. Engel, FEBS Lett. **529**, 65 (2002).
 - ¹³ K. Jagannathan, R. Chang, and A. Yethiraj, Biophys. J. **83**, 1902 (2002).
 - ¹⁴ G. G. Hsu, A. R. Bellamy, and M. Yeager, J. Mol. Bio. **272**, 362 (1997).
 - ¹⁵ H.-W. Wang, Y.-J. Lu, L.-J. Li, S. Liu, D.-N. Wang, and S.-F. Siu, FEBS Lett. **469**, 105 (2000).
 - ¹⁶ C.-C. Yin, M. L. Aldema-Ramos, M. I. Borges-Walmsley, R. W. Taylor, A. R. Walmsley, S. B. Levy, and P. A. Bullough, Mol. Microbiol. **38**, 482 (2000).
 - ¹⁷ M. J. Conroy, S. J. Jamieson, D. Blakey, T. Kaufmann, A. Engel, D. Fotiadis, M. Merrick, and P. A. Bullough, EMBO Reports **5**, 1153 (2004).
 - ¹⁸ D. L. Gibbons, M.-C. Vaney1, A. Roussel, A. Vigouroux, B. Reilly, J. Lepault, M. Kielian, and F. A. Rey1, Nature **427**, 320 (2004).
 - ¹⁹ C. Govaerts, H. Wille, H. B. Prusiner, and F. E. Cohen, Proc. Natl. Acad. Sci. USA **101**, 8342 (2004).
 - ²⁰ A. Kitmotto, N. Myronova, P. Basu, and H. Dalton, Biochem. **44**, 10954 (2005).
 - ²¹ D. L. Pagan and J. D. Gunton, J. Chem. Phys. **122**, 184515 (2005).
 - ²² M. P. Allen and D. J. Tildesley, *Computer simulation of liquids* (Clarendon Press, Oxford, 1987).
 - ²³ A. Daanoun, C. F. Tejero, and M. Baus, Phys. Rev. E **50**, 2913 (1994).